Flow and sediment suspension events over low-angle dunes: Fraser Estuary, Canada

R.W. Bradley,[1] J. G. Venditti,[1] R. A. Kostaschuk,[1] M. Church,[2] M. Hendershot,[1] and M. A. Allison[3]

Received 16 October 2012; revised 18 July 2013; accepted 20 July 2013.

[1] The morphodynamics of large sand-bedded rivers and estuaries are ultimately controlled by the way bed material is moved and the development of large, subaqueous sand dunes that control hydraulic flow resistance. It is widely thought that the primary mechanism for moving sandy bed material in these channels is large-scale coherent flow structures that cause suspension events whose properties vary with flow, especially in tidally influenced environments. Here, we examine mean flow and sediment suspension events over low-angle dunes (lee face angle $<30°$) in the unsteady flow of the Fraser Estuary, Canada. At high tide, flow nearly ceased and a salt wedge entered the channel, forcing salt water under the downstream-moving fresh water. The salt wedge persisted in the channel until late in the falling tide, causing stratification in the water column and instabilities along the saline-fresh water interface. At low tide, mean velocities peaked and forced the saline water out of the channel. Flow over the low-angle dunes displayed topographically induced patterns previously observed over high-angle dunes, but permanent flow separation was not observed. Large-scale sediment suspension events dominated sediment flux during low tide and became larger scale, yet less frequent, as the tide began to rise. The suspension events appeared to form over the lower stoss of the dunes and grew up over the bed forms and, less commonly, emerged downstream of the crest. Suspension events move ~69% of the total sediment in the flow above low-angle dunes when they are present.

Citation: Bradley, R. W., J. G. Venditti, R. A. Kostaschuk, M. Church, M. Hendershot, and M. A. Allison (2013), Flow and sediment suspension events over low-angle dunes: Fraser Estuary, Canada, *J. Geophys. Res. Earth Surf.*, *118*, doi:10.1002/jgrf.20118.

1. Introduction

[2] Most of our systematic understanding of sediment transport in sand-bedded rivers is based on steady uniform flows in controlled laboratory experiments. Yet a fundamental property of natural river channels is that flow fluctuates on scales ranging from hours (tides) to days (synoptic-scale floods) to months (annual snowmelt-dominated freshets) [*Venditti*, 2013]. The response of sand dunes to variable flows depends on the tractive and suspended bed material loads induced on and over dunes by the varying flow. There has been considerable research into dune morphological response to variable flows (see summary of early work in *Allen* [1982] and of more recent work in *Venditti* [2013]), but there have been far fewer studies of the suspended sediment dynamics over dunes under variable flow conditions. This limits our ability to construct realistic physical models of flow and sediment transport in low-land, sand-bedded river systems. Here, we describe the phenomena associated with the movement of bed material in a variable flow generated by tides. The eventual goal is to understand the dynamics of flow and large-scale suspension events over dunes, which dominate bed material transport in sand-bedded rivers [*Best*, 2005a, 2005b]. There have been several studies of suspension events in steady flows [e.g., *Kostaschuk and Church*, 1993; *Kostaschuk and Villard*, 1999; *Venditti and Bennett*, 2000; *Best*, 2005a; *Shugar et al.*, 2010]. Most have been qualitative in nature, and none has resolved the fundamental mechanisms for suspended sediment behavior under the varying flows that dominate in sand-bedded rivers near the sea.

[3] Fluid and sediment dynamics over dunes are controlled by dune geometry and whether the bed form is angle-of-repose asymmetric or low-angle symmetric [*Kostaschuk and Villard*, 1996, 1999; *Best and Kostaschuk*, 2002; *Best*, 2005a; *Venditti*, 2013]. Asymmetric dunes with long, gently sloping (2–6°) upstream stoss sides and short angle-of-repose (~30°) lee sides have been the traditional focus of research because they are easily produced in laboratories and frequently observed in

[1]Department of Geography, Simon Fraser University, Burnaby, British Columbia, Canada.
[2]Department of Geography, University of British Columbia, Vancouver, British Columbia, Canada.
[3]Institute for Geophysics, University of Texas at Austin, Austin, Texas, USA.

Corresponding author: R.W. Bradley, Department of Geography, Simon Fraser University, 8888 University Dr., Burnaby, BC V5A 1S6, Canada. (rwbradle@sfu.ca)

2169-9003/13/10.1002/jgrf.20118

small, shallow streams. However, growing numbers of field observations have shown that symmetrical dunes with similar stoss and lee lengths and smaller lee-side angles (<30°) are the preeminent bed forms in tidally influenced sand-bedded rivers and estuaries [*Smith and McLean*, 1977; *Kostaschuk and Villard*, 1996; *Roden*, 1998]. Observations of the fluid dynamics over low-angle dunes are limited to a few studies under steady flow [e.g., *Smith and McLean*, 1977; *Kostaschuk and Villard*, 1996; *Best and Kostaschuk*, 2002; *Shugar et al*., 2010]. These studies have revealed mean flow patterns similar to those well documented over high-angle dunes [e.g., *Nelson et al*., 1993; *McLean et al*., 1994; *Bennett and Best*, 1995; *Kostaschuk*, 2000; *Venditti and Bennett*, 2000; *Best*, 2005a; *Venditti and Bauer*, 2005], except that the well-known separation zone and counter-rotating eddy in the lee trough of high-angle dunes are notably absent [*Kostaschuk and Villard*, 1996], being replaced by a decelerated flow region that may experience highly intermittent near-bed flow reversal in the immediate lee region [*Best and Kostaschuk*, 2002].

[4] The time-dependent flow over dunes, regardless of whether they are low-angle or high-angle features, is dominated by large-scale, macroturbulent coherent flow structures that upwell through the water column where they may emerge at the surface as boils [*Jackson*, 1976; *Babakaiff and Hickin*, 1996; *Kostaschuk and Church*, 1993]. The form of macroturbulent structures over dunes has been variously described as (1) slowly rotating, upward tilting streamwise vortices [*Matthes*, 1947], (2) circular in shape with internal upwelling in the center and sharp boundaries marked by vortices [*Coleman*, 1969; *Jackson*, 1976], and (3) turbulent ejection events [*Kostaschuk and Church*, 1993; *Bennett and Best*, 1995]. *Babakaiff and Hickin* [1996] suggested that upwelling surface boils may appear as "roller structures" that have an axis of rotation in the downstream spanwise direction with ends that loop toward the center of the feature as "horns." Flume observations [*Nezu and Nakagawa*, 1993; *Müller and Gyr*, 1986] and observations of boils by *Best* [2005b] support the idea of a roller morphology; however, these authors suggest that they appear as vortex loops that have legs with a vertical spanwise axis of rotation in addition to a rotating head. This topology is entirely consistent with the large-eddy simulation by *Omidyeganeh and Piomelli* [2011] who show loop vortex evolution, growth, and upwelling toward the surface over a dune.

[5] *Matthes* [1947] originally referred to these structures as "kolks" and asserted that they have the potential to lift and move large volumes of bed material. Indeed, a series of investigations have since linked these macroturbulent structures to the suspension events that dominate bed material sediment transport in sand-bedded rivers [*Rood and Hickin*, 1989; *Kostaschuk and Church*, 1993; *Kostaschuk and Villard*, 1999; *Venditti and Bennett*, 2000; *Best*, 2005b; *Shugar et al*., 2010]. In tidal environments, macroturbulent eddies and the associated suspension events are not persistent features of the flow. They start to form when the tide begins to fall and channel discharge increases, and stop forming as high tide approaches and the channel discharge declines. Most previous work on these suspension events in tidal environments has focused on low-tide conditions, when they are assumed to be most energetic [*Kostaschuk and Church*, 1993; *Kostaschuk and Villard*, 1996]. Yet, it is not known where in the tidal cycle these features start to form, become most energetic, and stop forming. More importantly from a geomorphological perspective, it is not clear whether these structures transport more sediment at certain phases of the tidal cycle than at others. This information is critical to understanding how to integrate the effect of these suspension events over a tide cycle.

[6] Here, we address the following questions: (1) How does the flow structure over low-angle dunes change at different phases of the tide? (2) What are the characteristics of suspension events at various phases of the tide? (3) How much sediment is carried by suspension events? Understanding these dynamics is an important prerequisite to developing an understanding of why low-angle bed forms dominate in large, tidally influenced, sand-bedded rivers and estuaries and to improving the way suspension processes are represented in sediment transport models. We use acoustic Doppler current profiler transects to explore flow over low-angle dunes through semidiurnal tidal cycles in the main channel of the Fraser River Estuary, British Columbia, Canada. The analysis focuses on the mean flow structure and sediment suspension events, and how these change with tides.

2. Methods

2.1. Study Area

[7] Field observations were made in the main channel of the Fraser River Estuary near Steveston, British Columbia, Canada (Figure 1). The Fraser River discharges into the Strait of Georgia on the west coast of Canada, draining 234,000 km^2 of mountainous terrain. Mean annual river discharge at Mission (80 km upstream) is 3410 m^3/s with a mean annual flood of 9790 m^3/s [*McLean et al*., 1999]. Approximately 80% of the annual total discharge occurs during the spring snowmelt freshet between May and July [*Villard and Church*, 2003]. The lower reach of the river, near Steveston, is affected by mixed semidiurnal tides. At the mouth of the river, the mean tidal range is 3.1 m with extreme spring tides of over 5.4 m [*Villard and Church*, 2003]. This estuarine reach experiences a salinity intrusion that migrates upstream into the channel during rising tides and is forced downstream during falling tides. Median bed material grain size (D_{50}) in the estuary is 0.25 to 0.32 mm with little seasonal and spatial variation [*Kostaschuk et al*., 1989; *McLaren and Ren*, 1995]. Nine bed material samples collected using a grab sampler in the dune field shown in Figure 1 had a D_{50} of 0.27 mm.

2.2. Data Collection

[8] Three-dimensional (3-D) bathymetry and 3-D flow velocities were measured from the R/V *Lake Itasca* between 12 and 17 June 2010. Bathymetry was measured using a Reson 7101 Seabat Multibeam Echosounder (MBES), while 3-D flow velocities were simultaneously recorded using a Teledyne RD Instruments 1200 kHz Rio Grande Workhorse acoustic Doppler current profiler (aDcp). The MBES positioning was measured using a real-time kinematic GPS accurate to 0.01 m horizontally and 0.02 m vertically. The position of the aDcp was recorded using a GPS differentially corrected by a Canadian Coast Guard beacon about 1.70 km south of the dune field. The Differential Global Positioning System (DGPS) provides positioning with an accuracy of 0.25 m

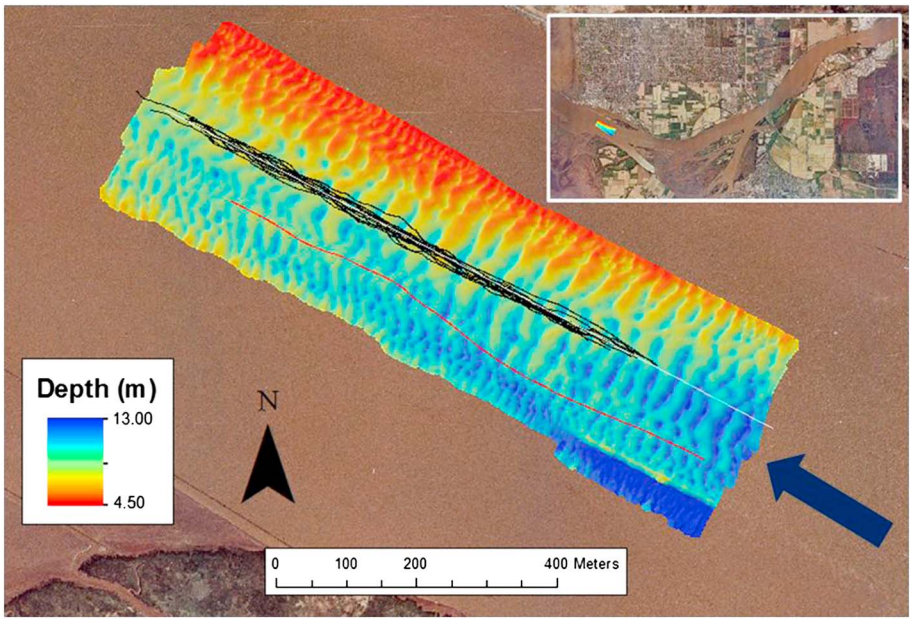

Figure 1. Bathymetric map of the study dune field (Survey G). Inset shows the position of the dune field in the main arm of the Fraser River, British Columbia. Black lines show the upstream-traveling aDcp lines, and the red line shows the downstream aDcp line (K2). The white line indicates the transect used to quantify dune morphology, and the blue arrow indicates flow direction.

horizontally and 0.50 m vertically. The manufacturer reported that depth resolution of the MBES is 1.25 cm [*Reson Inc.*, 2009]. The head generates 511 equidistant beams and measures relative water depths over a 150° wide swath perpendicular to the vessel track. Navigation, orientation, and attitude data (heave, pitch, and roll) were recorded using an Applanix POS MV V3 gyroscope inertial guidance system mounted inside the vessel.

[9] Three-dimensional flow velocities were measured on individual track lines at a vertical resolution of 0.25 m (vertical bin size) with the aDcp. Velocity is calculated relative to the instrument head; thus, measured velocities must be corrected by removing the vessel velocity as determined by bottom track (BT) or the GPS. Bottom tracking measures distance alongstream using the Doppler shift in frequency with respect to the bed. The aDcp provides velocity measurements with a

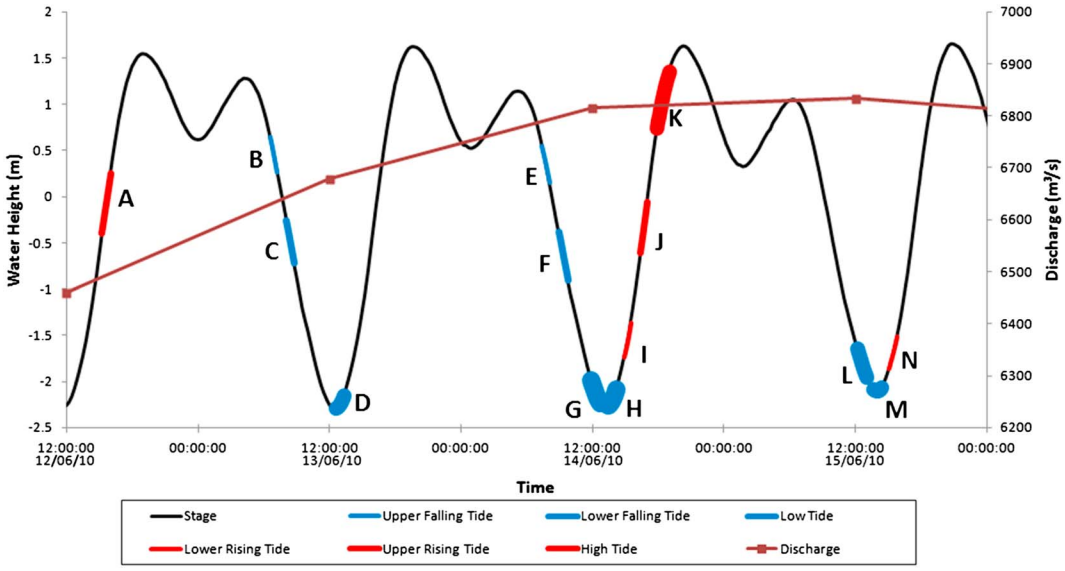

Figure 2. River stage (corrected to Geodetic Survey of Canada datum) at Steveston and discharge at Mission (80 km upstream of study reach) for the sampling period. Survey periods are marked by letters A–N. The 5 min averaged river stage data for Water Survey of Canada (WSC) station 08MH028 were provided by Lynne Campo of WSC (by request), and discharge data from WSC station 08MH024 are available online at http://www.wsc.ec.gc.ca (accessed on 2 August 2012).

Table 1. Descriptive Flow and Suspended Sediment Statistics for Each Transect Including Bed Velocity, References for Velocity Corrections, and the Availability of Vertical Velocity Data

Position in Tidal Cycle	Transect	Transect Time (s)	GPS Transect Length (m)	BT Transect Length (m)	v_{bed}[a] (m/s)	Reference Used	w[b]	$\langle u \rangle$ (m/s)	$\langle SSC \rangle$[c] (mg/L)	$\langle d \rangle$ (m)
Upper Falling	B	626	1024.7	1021.4	−0.005	BT	N	0.89	-	13.51
	E	556	981.7	969.3	−0.022	BT	N	0.93	-	13.53
Lower Falling	C	636	1011.1	985.3	−0.041	BT	N	1.45	-	12.85
	F	680	996.2	969.9	−0.039	BT	N	1.60	-	11.08
Low	L	839	994.5	1696.2	0.836	GPS	Y	1.95	439.87	11.45
	G	960	1017.3	2056.8	1.083	GPS	Y	2.20	413.20	11.06
	M	869	994.4	1801.0	0.928	GPS	Y	2.07	408.17	11.07
	D	795	1013.6	1751.8	0.928	GPS	Y	2.05	397.21	10.94
	H	787	977.3	1613.6	0.808	GPS	Y	1.97	372.75	10.89
Lower Rising	N	589	973.6	1173.6	0.340	GPS	Y	1.41	287.35	11.36
	I	461	976.6	1073.0	0.209	GPS	Y	1.23	211.31	11.53
Upper Rising	J	437	945.4	945.1	−0.001	BT	Y	0.30	55.25	12.59
	A	416	929.0	930.6	0.004	BT	Y	0.14	41.78	12.79
High	K	763	947.5	945.0	−0.003	BT	Y	0.13	30.58	13.99
	K2	578	984.6	995.0	0.018	BT	Y	−0.18	-	15.34

[a]Positive values indicate downstream direction, and negative values indicate upstream.
[b]Refers to the availability of vertical velocity data without contamination. See Figure 4 for further explanation.
[c]SSC is not calculated when salinity intrusion is present in the channel because calibration assumes zero salinity.

manufacturer-reported accuracy of ±0.5 cm/s and echo intensity with a precision of ±1.5 dB [*Teledyne RD Instruments*, 2001]. The aDcp was set to ping at 11 Hz, and pings were averaged in ensembles every 0.45 s to improve the signal-to-noise ratio. Average vessel velocity over the transects was about 1.54 m/s, resulting in profiles every 0.7 m. Averaging in the water column occurs over different volumes of water because each beam is oriented at an orthogonal angle of 20° in the vertical and beam spreading occurs at 1.5°.

[10] MBES and aDcp measurements of a dune field approximately 1 km long and 0.5 km wide (Figure 1) were made over multiple tidal cycles to see how flow and sediment transport changed with the tides. Figure 2 shows river stage at Steveston and daily mean discharge at Mission (~80 km upstream of study area) for the measurement period. Bed elevation and flow velocity measurements were made during 14 surveys over a 4 day period. Each survey consisted of five parallel streamwise transects that produced a continuous, overlapping bed map and five streamwise velocity transects. Individual surveys were grouped into "Upper Falling Tide," "Lower Falling Tide," "Low Tide," "Lower Rising Tide," "Upper Rising Tide," and "High Tide" according to their location within individual cycles to allow cross-cycle comparisons (Figure 2).

[11] ADcp results reported herein are from the centermost transect from each survey, over the most well-defined dunes measured, while the vessel was traveling upstream. Figure 1 shows the location of 15 transects over the dune field used in this analysis. Although, transects were measured with the boat moving in both the upstream and downstream directions, we included only the centermost upstream transect from each survey because the flow is then observed in a semi-Eulerian framework. This framework provides a nearly instantaneous view of large-scale sediment suspension events as they pass beneath the vessel and the spatial flow structure over the dunes as the boat moves over the bed. On downstream transects, the boat generally moved faster than the surface flow in order to maintain vessel control during high downstream velocities at lower tide stages. This obscured observations of suspension events and the mean flow structure by stretching them in the downstream direction to varying degrees depending on vessel velocity. Nevertheless, the observations are similar regardless of which direction the boat was moving. During the High Tide Survey K, aDcp results are reported from a transect (K2) that is south of the centerline while the boat was traveling up river (Figure 1). Flow was dominantly upstream during this transect so observations are still in a semi-Eulerian framework.

[12] Suspended sediment samples were collected on 17 June 2010 to calibrate aDcp backscatter to suspended sediment concentrations. A U.S. Geological Survey P-63 point-integrating suspended sediment sampler was opened for ~40 s at each of 0.1d, 0.2d, 0.4d, 0.6d, and 0.8d (where d = depth) to measure sediment concentrations. Three profiles were measured: one during Low Tide, one during Lower Rising Tide, and one at the Upper Rising Tide stages. Grain size of the samples was measured using a Sequoia LISST-Portable that uses laser diffraction to provide grain size distribution within a range of 1.9–381 μm. Filtration using 47 mm microfiber filters with a pore size of 1.6 μm was used to obtain sediment concentrations.

2.3. MBES and aDcp Processing

[13] Raw MBES data were imported into CARIS HIPS® software for postprocessing where lines and soundings were merged to produce bathymetric grids. This software allows for the removal of "bad pings" and corrections for changes in heave, pitch, and roll and tidal stage. The data were then imported into ArcGIS® and gridded at 1 m for further analysis of the bed surface and measurements of bed form characteristics. The processed bed surface maps were used to obtain bed profiles along aDcp transects because they provide a more accurate view of the bed than the aDcp, which averages depth over the four beam footprints. A streamwise transect that corresponded to the analyzed upstream-traveling aDcp transects was drawn through the bed form field of Survey G (Figure 1) to obtain all bed form measurements. We present dune morphological statistics from only one survey because spatial and temporal changes of dunes are beyond the scope of this study. Furthermore, there were no major changes in bed configuration over the measurement period.

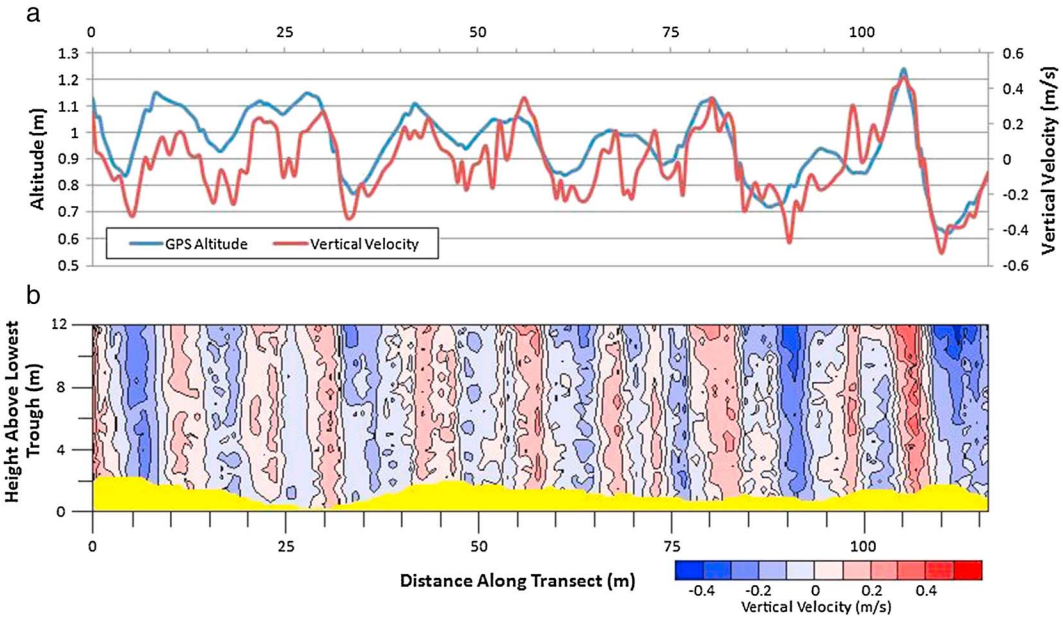

Figure 3. (a) The influence of altitude change on vertical velocity measurements along an equidistant row across the top of the profiles. (b) Contour map of the vertical velocity flow field showing contamination from altitude change.

[14] A software package developed by Colin Rennie (University of Ottawa) [e.g., *Rennie and Rainville*, 2006; *Rennie et al*., 2007; *Rennie and Church*, 2010] was used to extract the aDcp data and correct for the magnetic variation, depth of the transducer below the surface, and height of the GPS receiver above the instrument. The Rennie software also allows correction of measured velocities by removing the vessel velocity referenced by the DGPS (v_{DGPS}) or bottom tracking (v_{BT}). Bottom track should be limited to immobile bed conditions as a mobile bed produces bias in the measured frequency of the Doppler shift because the shift is related to both the boat and bed velocities. This bias allows for an estimate of apparent bed velocity (v_{bed}) as

$$v_{bed} = v_{DGPS} - v_{BT}. \quad (1)$$

[15] We chose to use bottom tracking when the estimated bed velocity was near the range of the instrument error because some of the velocity data experienced "gaps" when the DGPS was used as a reference. Transects included in our analysis that used the DGPS as a reference did not experience DGPS failure and thus were not contaminated. Estimated bed velocity for each transect as well as the reference used to calculate velocities is reported in Table 1.

[16] Velocity records were also periodically and variably affected by large persistent surface waves that caused "up and down" vertical vessel motion. Figure 3 shows an example from Transect E with a particularly strong influence of vertical vessel motion on reported vertical velocities. Apparent vertical velocity reported along a horizontal plane near the surface should show limited variation; however, the vertical velocity fluctuates in an up and down motion that roughly corresponds to the changes in vessel altitude as recorded by the DGPS (Figure 3a). This issue resulted in contaminated vertical flow field maps (Figure 3b) for some of the transects. Attempts to remove the altitude signal from the vertical velocity records by taking the derivative of the altitude in the time domain and correcting for lags between the signals were unsuccessful because the lags were inconsistent and vertical velocity response to altitude changes varied in strength. As a result, there were no useful vertical velocity measurements during the Upper Falling and Lower Falling transects (Table 1), and so, they were not included in the analysis. The remaining transects showed minimal contamination from the changes in altitude of the boat and thus were included in this analysis. Nonetheless, care must be taken when interpreting vertical velocities recorded from an aDcp on a moving vessel.

2.4. Calibration of aDcp Backscatter to Suspended Sediment Concentrations

[17] Echo intensity (EI) recorded in counts can be used to estimate the concentration of suspended sediment in a wide range of flows [*Topping et al*., 2007; *Domarad*, 2011; *Attard*, 2012]. Backscatter strength is a function of sediment particle size, type, and concentration; thus, backscatter is directly proportional to concentration for a constant sediment type and size [*Topping et al*., 2007; *Wright et al*., 2010]. In this study, EI was converted to total suspended sediment concentration using the calibration methodology developed by *Topping et al*. [2007] which corrects for both water and sediment absorption. The first step in this calibration is to convert the EI recorded by the aDcp into measured backscatter:

$$MB = sf \times EI, \quad (2)$$

where sf is a beam-specific echo intensity-scale factor obtained from RD Instruments. The forward facing beam was selected for this analysis, which has sf = 0.383 dB/count. Changes in backscatter through the water column may be

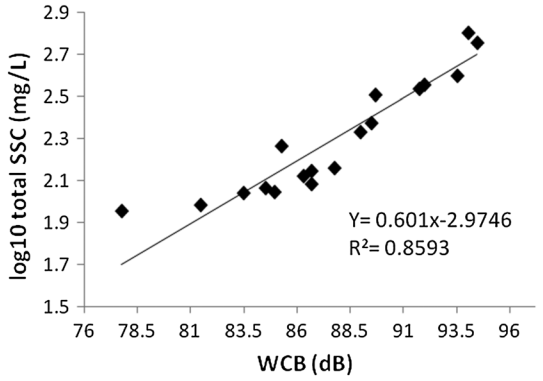

Figure 4. Calibration curve of suspended sediment concentrations (SSC) with water-corrected backscatter (WCB). The fitted line has been corrected using the reduced major axis correction [see *Mark and Church*, 1977] because it is a formal calibration.

caused by water absorption and beam spreading; thus, water-corrected backscatter (WCB) is calculated as

$$\mathrm{WCB} = \mathrm{MB} + 20\log_{10}R + 2a_wR, \tag{3}$$

where R is the distance along the beam to each cell and a_w is the water absorption coefficient. Assuming zero salinity, a_w is calculated [*Schulkin and Marsh*, 1962] as

$$a_w = 8.686 \times 3.38 \times 10^{-6}\frac{f^2}{f_T} \tag{4}$$

$$f_T = 21.9 \times 10^{\left[6-\frac{1520}{T+273}\right]}, \tag{5}$$

where f is the frequency of the aDcp and T is the water temperature in °C. Suspended sediment concentration (SSC) is calculated from the sonar equation for sound scattering from small particles [*Gartner*, 2004]:

$$\log(\mathrm{SSC}) = a + b \times \mathrm{WCB}, \tag{6}$$

where a and b are the intercept and slope from a regression between WCB and measured suspended sediment concentrations. Water-corrected backscatter WCB values from the same depth as the P-63 samples were selected to correlate with suspended sediment concentration (Figure 4). This regression analysis produced a WCB calibration as

$$\mathrm{SSC} = 10^{0.0601(\mathrm{WCB})-2.9746}, \tag{7}$$

with a R^2 value of 0.86, suggesting that it is a good means of estimating total suspended sediment. *Topping et al*. [2007] and *Wright et al*. [2010] extend their method to discriminate silt and clay from suspended sand concentrations. We attempted the analysis but found that silt and clay concentrations were poorly and negatively correlated with the sediment attenuation coefficient. The *Topping et al*. [2007] and *Wright et al*. [2010] method was developed for a side-facing aDcp where sediment concentration does not vary along the aDcp beams. Correlation with the sediment attenuation coefficient may not be appropriate when suspended sediment concentrations and grain size increase toward the bed, so we did not pursue acoustic grain size separation.

2.5. Examination of Flow Structure Over Low-Angle Dunes

[18] Spatially averaged downstream velocity $<u>$ values for entire flow fields were calculated as

$$u = \frac{\sum_{x=1}^{n_x}\sum_{y=1}^{n_y}u}{n}, \tag{8}$$

where n_x is the number of horizontal planes, n_y is the number of vertical planes, n is the number of measurements in the field, and u is the at-a-point downstream velocity. Angle brackets indicate a spatial average. However, $<u>$ reveals nothing about the flow structure over the dunes. Two-dimensional plots of mean velocity over dunes also reveal little about the spatial flow structure beyond topographically forced acceleration over the stoss and deceleration over the lee because velocity generally increases logarithmically above the bed. A more effective method to identify spatial patterns is to calculate the deviation from $<u>$ and the spatially averaged vertical velocity $<w>$. We can calculate the deviation as the instantaneous velocity at a location minus the spatial mean $<u>$ or by calculating the mean velocity along horizontal equidistant planes at 0.25 m intervals (bin spacing) from the water surface and subtracting the calculated mean from the instantaneous velocities along the plane. For the latter, mean horizontal velocity $<u>_x$ and mean vertical velocity $<w>_x$ are calculated for each horizontal plane in the vertical as

$$\langle u\rangle_x = \frac{\sum_{x=1}^{n}u}{n_{ix}} \tag{9}$$

$$\langle w\rangle_x = \frac{\sum_{x=1}^{n}w}{n_{ix}}, \tag{10}$$

where n_{ix} is the number of at-a-point measurements within the plane. The calculated $<u>_x$ and $<w>_x$ were then used to calculate the deviations in u and w for each plane as

$$u'_x = u - u_x \tag{11}$$

$$w'_x = w - w_x. \tag{12}$$

[19] Figure 5 shows contour maps of velocity deviation from $<u>$ (Figure 5a) and $<u>_x$ (Figure 5b). The velocity deviation from $<u>$ is obscured by the general decline in velocity toward the bed, preventing any more detailed interpretation of the flow structure. Calculation of the velocity deviation from $<u>_x$ reveals a more subtle structure, so we use this type of deviation in our analysis.

[20] In calculating the spatial averages and deviations, and in our analyses and interpretations of the data, we used the full length of each transect, but we cannot effectively present the full ~1 km long transects in our plots. Therefore, we have selected 100 m long sections of the data over the largest dunes in the field to display the relevant properties of the flow. We also calculated the spatial averages over these shorter distances to determine if the observation window length affects our results and found that it does not significantly affect the patterns we observe.

2.6. Examination of Sediment Suspension Over Low-Angle Dunes

[21] Water-corrected backscatter and suspended sediment concentration patterns over dunes were highly variable, so

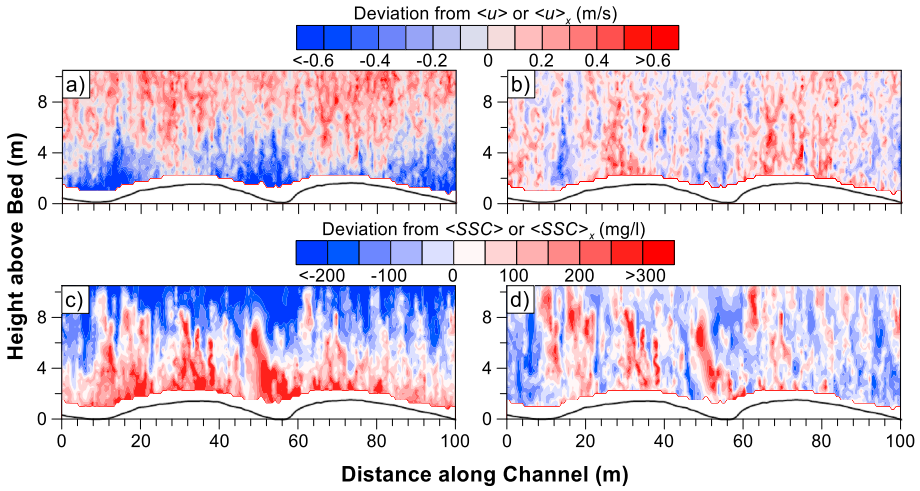

Figure 5. (a) Deviation in downstream velocity from the mean value of the entire flow field (u'). (b) Deviation in downstream velocity from the mean value along horizontal planes equidistant below the water surface (u'_x). (c) Deviation in suspended sediment concentration from the mean value of the entire flow field (SSC′). (d) Deviation in suspended sediment concentration from the mean value along horizontal planes equidistant below the water surface (SSC′$_x$). River flow is right to left. Vertical exaggeration is 3x.

spatially averaged mean values for the whole field were calculated as

$$\langle \mathrm{WCB} \rangle = \frac{\sum_{x=1}^{n_x} \sum_{y=1}^{n_y} \mathrm{WCB}}{n} \tag{13}$$

$$\langle \mathrm{SSC} \rangle = \frac{\sum_{x=1}^{n_x} \sum_{y=1}^{n_y} \mathrm{SSC}}{n}, \tag{14}$$

where WCB is at-a-point water-corrected backscatter and SSC is at-a-point suspended sediment concentration. Deviations from the mean water-corrected backscatter WCB′ and mean suspended sediment concentration SSC′ were calculated as

$$\mathrm{WCB}' = \mathrm{WCB} - < \mathrm{WCB} > \tag{15}$$

$$\mathrm{SSC}' = \mathrm{SSC} - < \mathrm{SSC} > . \tag{16}$$

[22] SSC′ contour maps provide a nearly instantaneous view of suspended sediment transport patterns. We also calculated spatial mean $<\mathrm{WCB}>_x$ and mean $<\mathrm{SSC}>_x$ for each horizontal plane in the vertical as

$$\mathrm{WCB}_x = \frac{\sum_{x=1}^{n} \mathrm{WCB}}{n_{ix}} \tag{17}$$

$$\mathrm{SSC}_x = \frac{\sum_{x=1}^{n} \mathrm{SSC}}{n_{ix}} \tag{18}$$

in order to examine mean profiles along transects.

[23] We focus our interpretation and analysis on SSC′ and WCB′ values rather than deviations from $<\mathrm{WCB}>_x$ and mean $<\mathrm{SSC}>_x$ because the former captures the structure of suspension events, which originate at the bed and are responsible for the concentration gradient. Comparison of SSC′ (Figure 5c) and deviation from $<\mathrm{SSC}>_x$ (Figure 5d) values shows that the same structures are apparent, but the form of the structure in the lower portion of the flow and some weaker structures are eliminated in Figure 5d. As with the velocity data, we present 100 m long sections of the data over the largest dunes in the field as examples of the sediment transport field, but our analysis and interpretation of the data consider the full ~1 km long transects at each phase of the tide. Note that we cannot reliably distinguish between variability in SSC and backscatter caused by density gradients between saline and fresh water. This limits our ability to calculate SSC over low-angle dunes to periods when there is no salt water in the channel at Low, Lower Rising, and Upper Rising tidal phases (Table 1).

2.7. Identification of Flow Structures and Sediment Suspension Events

[24] aDcp beam geometry and measurements from a moving vessel limit observations of turbulence in our velocity measurements. Sampling volume increases with depth because beams are oriented at 20° off vertical and beam spreading occurs at 1.5°. The average distance of 0.71 m between measured ensembles caused by boat motion adds to the sampling volume. These factors create sampling diameters of 2.23 m at 2 m below the surface, 5.26 m at 6 m, and 9.80 m at 12 m. In order to identify coherent flow structures in the velocity records, they would have to be larger than these sampling volumes. Because of this, coherent flow structures are not obvious in most of the velocity data. However, sediment suspension events are clearly defined in the SSC′ records because we selected only the forward facing beam to reduce the sampling volume. SSC measurements occur over much smaller sampling diameters of 0.76 m at 2 m below the water surface, 0.87 m at 6 m, and 1.02 m at 12 m.

3. Results

3.1. Dune Characteristics

[25] Dune profile geometry and three dimensionality varied both spatially and temporally over the measurement period. Individual bed forms changed through the tidal cycles because of active dune migration during unstratified flow around low tide. The bathymetric maps (e.g., Figure 1) also reveal the presence of bar topography on the northern channel bank.

Table 2. Morphological Characteristics of Dunes Along Transect in Survey G (Figure 1)

	Height	Length	Steepness	Symmetry	Lee Side Slope	Stoss Side Slope
	H (m)	L (m)	H/L	L_{smm}	a_l (deg)	a_s (deg)
Mean	1.49	37.29	0.04	1.20	11.9	5.2
Max	2.39	51.94	0.08	2.00	21.9	9.3
Min	0.72	12.98	0.02	0.41	3.3	1.0

Dunes generally increased in size as they moved over the bar, consistent with observations by *Villard and Church* [2003]. Summary statistics in Table 2 are from 18 well-defined dunes with heights that exceeded 0.5 m. The mean lower lee-side slope of the dunes was about 12°, typical of low-angle dunes in large rivers [e.g., *Smith and McLean*, 1977; *Kostaschuk and Villard*, 1996; *Roden*, 1998], and mean symmetry L_{sym} (stoss length divided by lee length, separated at the crest) was 1.20. A perfectly symmetrical dune has $L_{sym} = 1.0$, and an asymmetric "angle-of-repose" dune (assuming a height and length of the dunes observed here) has $L_{sym} = 14.4$. None of the bed forms displayed the lee-side angle-of-repose (>30°) geometry typical of high-angle dunes (maximum observed being 22°). These dune characteristics were similar to the low-angle dunes previously observed by *Kostaschuk and Villard* [1996] in this reach of the Fraser River.

3.2. Mean Flow and Suspended Sediment Concentrations

[26] Table 1 summarizes $<u>$, spatially averaged flow depth $<d>$, and <SSC> along the transects. At High Tide, downstream flow in the channel nearly stopped; $<u>$ reached the lowest measured point of 0.13 m/s (Transect K) with evidence of weak upstream flow (Transect K2). As the tide began to fall (Transects B and E), $<u>$ was ~0.9 m/s and continued to accelerate with the falling tide (Transects C and F). During Low Tide transects (L, G, M, D, and H), $<d>$ approached a minimum of ~11 m and $<u>$ peaked at 2.20 m/s. The peak in $<u>$ preceded the lowest $<d>$, suggesting that depth response to tidal change lagged behind velocity. The maximum recorded <SSC> of ~440 mg/L occurred during the first Low Tide transect (L), and higher <SSC> generally occurred when transects were taken earlier in the Low Tide phase. Maximum $<u>$ lagged behind the peak in <SSC>, suggesting that a large supply of finer bed material was transported out of the channel early in the tidal fall and that less sediment was readily available for transport when $<u>$ peaked. The easily eroded material likely represents fine sediment that settled to the bed during the near slack water at high tide. Transects taken later in the Low Tide phase had lower <SSC> as less fine sediment was readily available for transport and flow velocities began to slacken. On the rising tide, $<u>$ steadily decelerated from ~1.2 m/s during the Lower Rising tide transects (N and I) to ~0.2 m/s during the Upper Rising tide transects (J and A). Early in the Rising Tide (Transects N and I), <SSC> continued to decrease as $<u>$ decreased. As tides approached maximum height, <SSC> was relatively low.

[27] Examination of our bed material grain size distributions indicates that the D_{10} is 155 µm. This is often used as a division between bed material and wash load under the assumption that the finest 10% of the bed material is wash load trapped by flow through the bed sediments. Accepting this division, wash load accounts for 68% of the total load at low tide, 74% on the rising tide, and 93% at high tide. The pattern suggests that, at low tide, bed material transport contributes substantially to the total sediment flux in the river.

[28] These mean flow and suspended sediment concentration patterns arise because of the dynamic interaction of fresh and saline water in the estuary that can be appreciated by examining the vertical profiles of velocity, backscatter, and suspended sediment concentration. Figure 6 shows profiles of $<u>_x$, $<WCB>_x$, and $<SSC>_x$ for transects within the different phases of the tidal cycle. We show both $<WCB>_x$ and $<SSC>_x$ because $<SSC>_x$ cannot be reliably calculated when saline water is present in the channel. However, $<WCB>_x$ reveals the saline-fresh water interface in the channel and may also reflect patterns in suspended sediment concentrations.

[29] Early in the tidal fall (Upper Falling Tide, Figure 6a), the salt wedge intrusion was evident in the lower portion of the profile, causing stratification in the flow. A pycnocline, recorded as a peak in backscatter due to the sharp density gradient between the fresh and saline water [*Geyer and Farmer*, 1989; *Tedford et al.*, 2009; *Kostaschuk et al.*, 2010], is obvious in the vertical profile of $<WCB>_x$ from 9 to 11 m above the bed. Downstream velocity $<u>_x$ was greatest in the upper fresh water layer but sharply declined below the pycnocline. Below 7 m above the bed, velocity was constantly small, yet positive, indicating that the wedge was no longer migrating upstream and was beginning to retreat from the channel. This highly stratified flow pattern no longer occurred as the tides continued to fall on the Lower Falling Tide (Figure 6b); $<u>_x$ decreased more gradually from the surface to ~7 m where there was a sharp kink in the profile typical of spatially averaged flow over dunes [*Smith and McLean*, 1977; *McLean et al.*, 1994; *McLean et al.*, 1999]. There is no obvious pycnocline in vertical profiles of $<WCB>_x$, but it is entirely possible that pockets of saline water, as observed by *Geyer and Farmer* [1989] on falling tide, may be in the channel; thus, we do not calculate SSC values. The value of $<WCB>_x$ increased from the surface linearly to ~6 m where there was a weak kink in the profile, suggesting that bed material resuspension was contributing to WCB in the lower profile.

[30] During Low Tide (Figure 6c), when downstream velocity was highest in the cycle, velocity profiles exhibited shapes typical of steady flow over dunes. Mean downstream velocity $<u>_x$ decreased relatively slowly from the surface to 3.5 m above the bed where there was a distinct kink in the velocity profile. This sharp decrease in $<u>_x$ occurred within the range of the maximum and minimum bed height and illustrates the strong influence of bed form morphology on the mean downstream flow. Investigation of individual dune troughs showed no negative downstream velocity, suggesting that flow separation was not present in the field, although the aDcp beam geometry makes measurements of

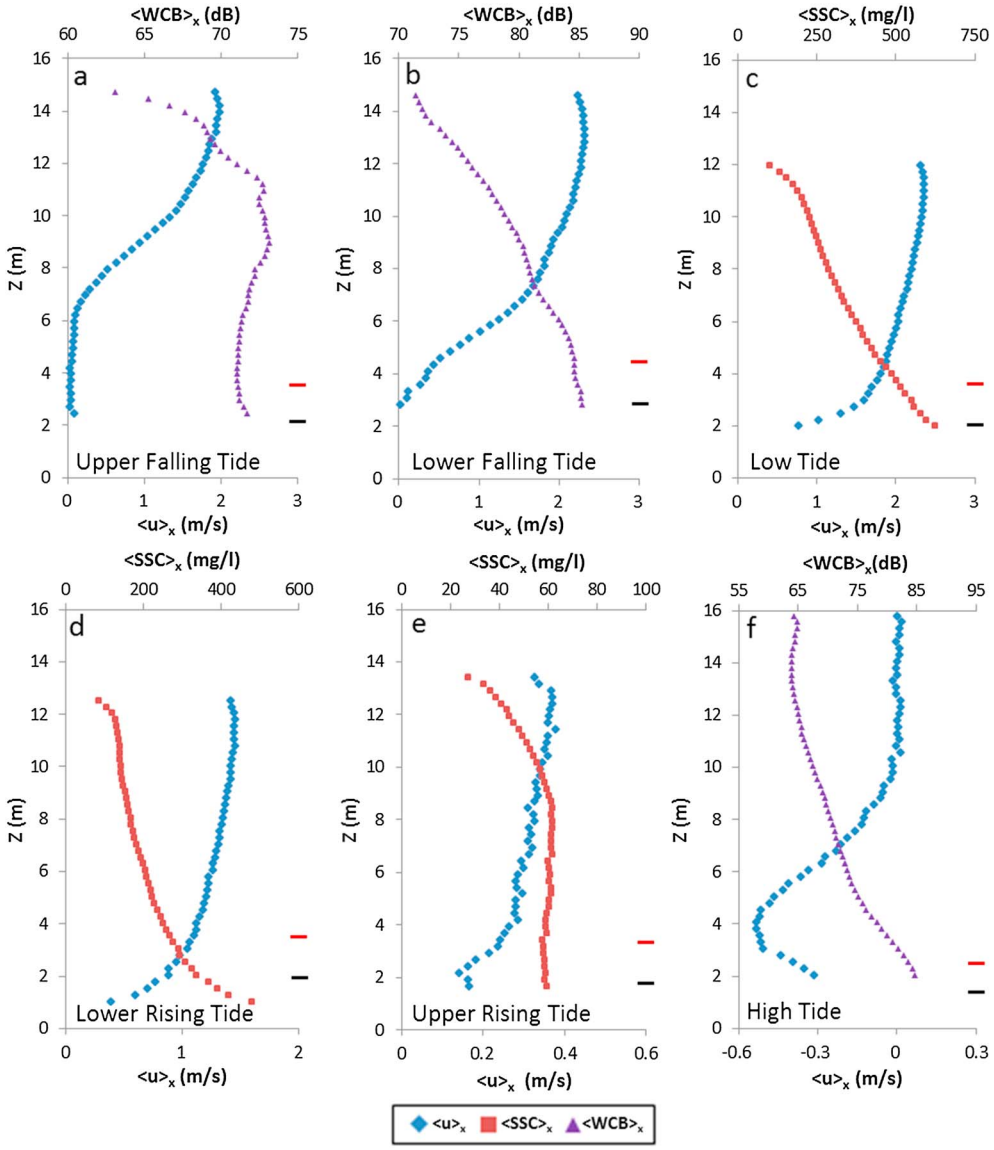

Figure 6. Mean downstream velocity ($<u>_x$), suspended sediment concentration ($<SSC>_x$), and/or water-corrected backscatter ($<WCB>_x$) above the lowest bed point for select transects within the defined tidal cycle periods. (a) Upper Falling Tide (Transect B), (b) Lower Falling Tide (Transect F), (c) Low Tide (Transect H), (d) Lower Rising Tide (Transect I), (e) Upper Rising Tide (Transect J), and (f) High Tide with Salinity Intrusion (Transect K2). Red ticks indicate the highest bed point along the transect, while black ticks show the average bed position.

near-bed velocity difficult. The vertical profile of $<SSC>_x$, had a weak sigmoidal shape, typical of equilibrium suspended sediment concentration profiles, reflecting the decrease in turbulent sediment suspension capacity above the bed in unstratified flow [*Kostaschuk and Villard*, 1999; *Kostaschuk*, 2000; *Shugar et al*., 2010]. As the tide began to rise (Lower Rising Tide, Figure 6d), the $<u>_x$ profiles displayed similar shapes to Low Tide profiles but had a smaller range in values and a less-defined, near-bed kink when compared to the Low Tide profiles (Figure 6c). The $<SSC>_x$, profiles were more strongly sigmoidal. As tides approached the maximum stage in the Upper Rising Tide transects (Figure 6e), $<u>_x$ displayed little variation, except below ~4 m above the bed where velocity decreased into the dune troughs. Suspended sediment concentrations were constant at ~55 mg/L throughout much of the profile, but at 9 m above the bed, concentration began decreasing to about 20 mg/L at the surface.

[31] Later, during the High Tide transects (Figure 6f), the salt wedge intrusion entered the channel as indicated by the negative $<u>_x$ from ~9 m to the bed. The structure of the wedge is better appreciated when the downstream velocity as recorded by the aDcp is examined along the whole transect (Figure 7). At the head of the salt wedge (Figure 7, 700 m), velocity ranges from about −0.3 to −0.6 m/s (upstream flow), but further downstream, within the salt wedge, velocity approaches −1.5 m/s. The decreased upstream velocity at the head of the wedge was likely due to the resistance from the downstream-flowing fresh water and the bed roughness. Velocity within the wedge over bed forms is more negative than that over the troughs because topographic forcing

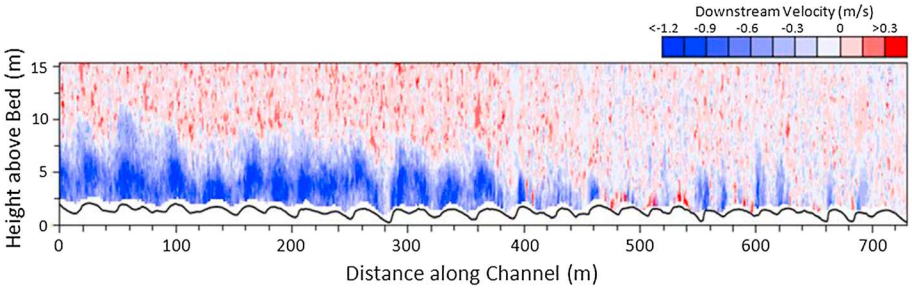

Figure 7. Downstream velocity for High Tide (Transect K2). River flow is right to left. Vertical exaggeration is 3x.

caused the saline water to accelerate over dune crests and decelerate in the troughs. Regions of negative downstream velocity appear as plumes over dunes as they are topographically lifted toward the surface (Figure 7). Higher up in the water column, these plumes were tilted in the downstream direction as they mixed with the slowly moving, downstream-directed fresh water above. There is no evidence of a pycnocline in the $<WCB>_x$ profile (Figure 6f). Values of $<WCB>_x$ within the upper fresh water remained relatively constant but increased toward the bed due to the presence of the salt wedge. This suggests that flow was heavily mixed as the salt wedge entered the channel, preventing a sharp gradient from forming. It has been suggested that this occurs because mixing between the wedge and the fresh water is heightened by the presence of dunes along the boundary [cf. *Kostaschuk et al.*, 2010].

3.3. Spatial Flow Structure Over Dunes

[32] Figure 8 shows the spatial pattern of streamwise velocity deviation from the mean u'_x for different sections of the tidal cycle. Figure 9 shows the patterns of vertical velocity deviation from the mean w'_x for Low Tide, Low Rising Tide, and Upper Rising Tide. We present vertical velocity contour maps for only these tidal phases because observations at other phases were contaminated by waves that caused vertical vessel motion. We have selected sections of transects over the largest dunes in the channel for display purposes, but the patterns are consistent along the full length of the transects at each phase in the tide. During the Upper Falling Tide, u'_x showed no coherent patterns over the dunes (Figure 8a). River flow began to dominate in the channel as the tide continued to fall, flushing out the salt wedge and removing the highly stratified flow structure, creating larger values of u'_x than previously observed in the tidal cycle (Figure 8b, −0.65 to +0.80 m/s). A larger u'_x range, especially near the boundary, suggests that the bed began to influence the flow as increased resistance added variability in the velocity that was not observed earlier in the tidal fall. Flow over larger bed forms (Figure 8b, 50 to 75 m) began to show weak evidence of topographical forcing as the fluid accelerated over the crestal region and decelerated due to expansion in the trough.

[33] During Low Tide observations (Figure 8c), streamwise velocity deviation u'_x ranged from −0.80 to 0.80 m/s and generally displayed patterns consistent with topographical forcing. Well-defined regions of slow downstream flow occurred in dune troughs, extending from the lower lee to the lower stoss where flow accelerated up the stoss (Figure 8c, 50–70 m). The largest positive u'_x frequently occurred along the stoss and at the crest where flow converges (Figure 8c, 65–90 m).

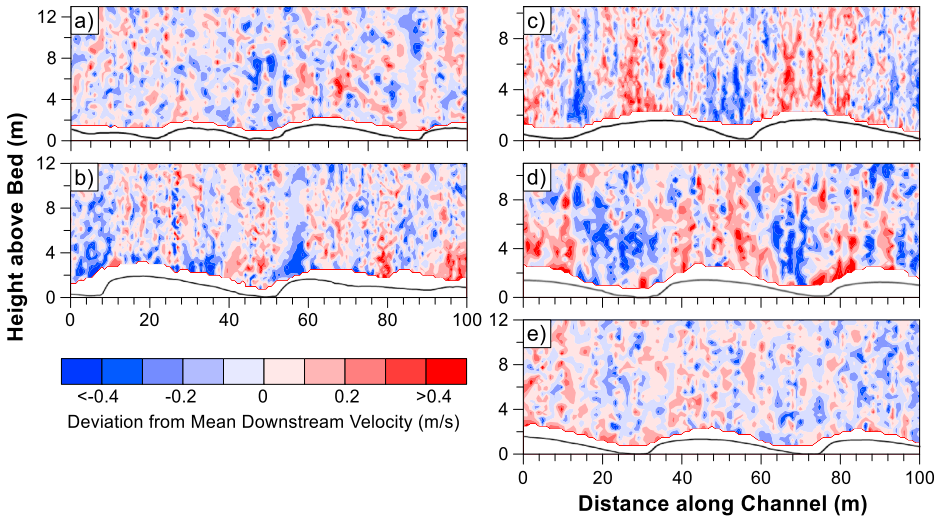

Figure 8. Deviation in downstream velocity from the mean (u'_x) for (a) Upper Falling Tide (Transect B), (b) Lower Falling Tide (Transect F), (c) Low Tide (Transect H), (d) Lower Rising Tide (Transect I), and (e) Upper Rising Tide (Transect J). High Tide is not included because there was an alongstream velocity gradient that dominated the signal. River flow is right to left. Vertical exaggeration is 3x.

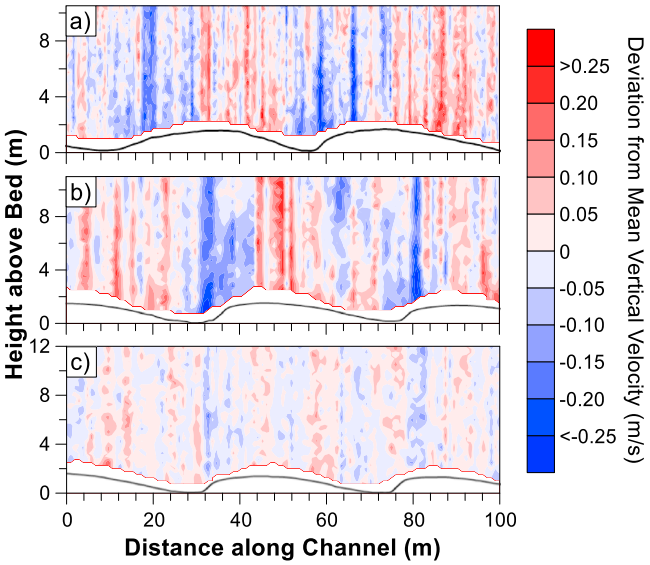

Figure 9. Deviation in vertical velocity from the mean (w'_x) for (a) Low Tide (Transect H), (b) Lower Rising Tide (Transect I), and (c) Upper Rising Tide (Transect J). River flow is right to left. Vertical exaggeration is 3x.

The largest range in u'_x appeared lower in the flow, revealing a strong influence of the bed. Upwelling occurred as fluid converged and was forced up over the bed forms beginning at the trough and extending toward the crest. Downwelling occurred after the crest and in the lee of the bed forms (Figure 9a).

[34] During Lower Rising Tide, the spatial pattern in u'_x was consistent with the topographical forcing observed during the Low Tide transects, although the range in u'_x was smaller (Figure 8d, −0.60 to +0.60 m/s). Regions of downstream-tilted decelerated flow emerged out of the troughs and over the stoss of dunes (Figure 8d). As the decelerated downstream fluid moved over the dunes, it was ramped up into the flow when it entered the zone of positive vertical velocity. As the tide continued to rise, patterns in the velocity records were less apparent. Streamwise velocity deviations from the mean u'_x (Figure 8e) were low at −0.5 to +0.5 m/s and were highly variable. Clear evidence of upwelling and downwelling due to topographic forcing no longer appeared in the vertical velocity records (Figure 9c).

3.4. Suspension Events Over Low-Angle Dunes

[35] Figure 10 shows mean water-corrected backscatter deviation from the mean WCB′, and Figure 11 shows the suspended sediment concentration deviation from the mean SSC′ over dunes for the different phases of the tidal cycle. As with the velocity contour maps presented above, we have

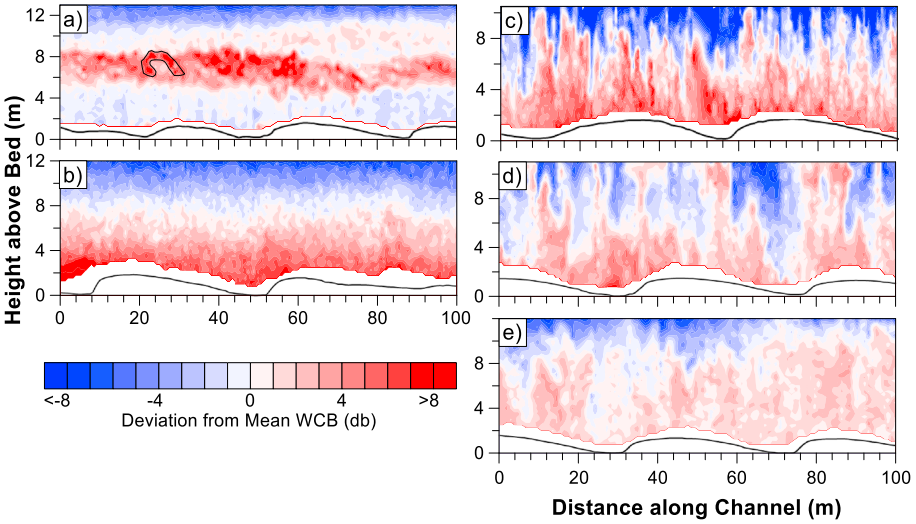

Figure 10. Deviation in water-corrected backscatter from the mean (WCB′) for (a) Upper Falling Tide (Transect B), (b) Lower Falling Tide (Transect F), (c) Low Tide (Transect H), (d) Lower Rising Tide (Transect I), and (e) Upper Rising Tide (Transect J). The black line in Figure 10a highlights a well-defined interfacial wave that cusped up into the freshwater layer. River flow is right to left. Vertical exaggeration is 3x.

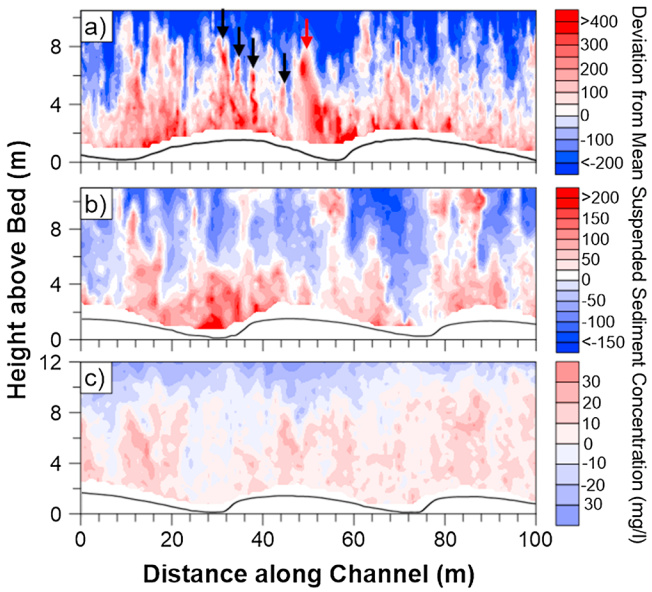

Figure 11. Deviation in suspended sediment concentration from the mean (SSC′) for (a) Low Tide (Transect H), (b) Lower Rising Tide (Transect I), and (c) Upper Rising Tide (Transect J). Note the changing SSC′ color scale between tidal positions. The black arrows in Figure 11a highlight a series of suspension events that emerged over the stoss and grow toward the surface over the crest, and the red arrow indicates a suspension event that appeared over the lee. River flow is right to left. Vertical exaggeration is 3x.

selected sections of transects over the largest dunes in the channel for display purposes, but the patterns are consistent along the full length of the transects at each phase in the tide. During the Upper Falling Tide observations, the density interface is well defined (Figure 10a) and peaks in WCB′ values along the interface provide evidence of interfacial waves about 10 m in length and 2 m in height that cusped up into the freshwater layer and propagated downstream (Figure 10a). However, there is no evidence of suspension events. WCB′ was larger during the Lower Falling Tide than during the Upper Falling Tide, and positive WCB′ dominated the lower half of the water column (Figure 10b). This reflects a combination of saline water [e.g., *Geyer and Farmer*, 1989] and increased SSC that was trapped in these regions of lower downstream flow velocity. The source of the sediment was likely fine sediment deposited at high tide as previously suggested by *Kostaschuk and Best* [2005]. The lack of well-defined individual suspension events in the records during the Lower Falling Tide is conspicuous because it appears that their absence suppressed sediment concentrations higher in the water column.

[36] During Low Tide observations, well-defined suspension events emerged that were spatially variable but exhibited consistent patterns over individual dunes that are highlighted in the examples presented in Figures 10c and 11a. These suspension events appear in the WCB′ records (Figure 10c), but we can examine the actual deviations from the mean sediment concentrations in Figure 11a because of the absence of saline water. Suspended sediment concentration deviation from the mean ranged from −310 to 625 mg/L (Figure 11a). Numerous narrow zones of high SSC′ rose up into the water column from the bed and extended to the surface. Values of SSC′ within individual events were highly variable with some of the better defined events (Figure 11a, 32 and 52 m) deviating by up to 600 mg/L from the mean, which is 2.5 times <SSC>. Values of SSC′ between individual events dropped to as little as 15% of <SSC>. Numerous suspension events formed over individual dunes, making it difficult to distinguish between events and to determine their origins in relation to the dunes, although they tended to emerge at the lower to midstoss region and over the lee of the bed forms. Suspension events appeared low in the water column over the lower stoss but increased in height as they moved over the dune until reaching near the surface downstream of the crest. These structures grew up into the flow at a mean of 24° with a range from 9 to 42°. Other large events, such as at 52 m in Figure 11a, emerged over the lower lee and trough. Flow characteristics of individual suspension events were not well captured in the velocity records (Figure 8c), but larger positive deviations in SSC′ frequently coincided with zones of larger negative u'_x.

[37] As the tide rose during Lower Rising Tide phase, SSC′ decreased from the previous phase (Figure 11b, −145 to +190 mg/L), but easily identifiable large-scale suspension events were apparent in the WCB′ (Figure 10d) and SSC′ (Figure 11b) records near the bed that maintained their shape toward the surface. The structures appeared less frequently than events observed during Low Tide but similarly grew up into the flow at a mean of 25° and a range from 14 to 42°. Strong positive SSC′ occurred at the lower stoss where structures grew above the bed until reaching the flow surface over the bed form upper stoss or crest (Figure 11b, 56 to 70 m). Some events emerged at the crest and lower lee, although they were less frequent than those observed at low tide. Bed form troughs and lee sides often displayed large concentrations of suspended sediment near the bed (Figure 11b, 20 to 40 m).

[38] As downstream velocity in the channel decelerated during the Upper Rising Tide, patterns in the velocity and suspended sediment records were less apparent. Values of SSC′ ranged from −33 to +49 mg/L (Figure 11c) with weak evidence of the suspension events that dominated the

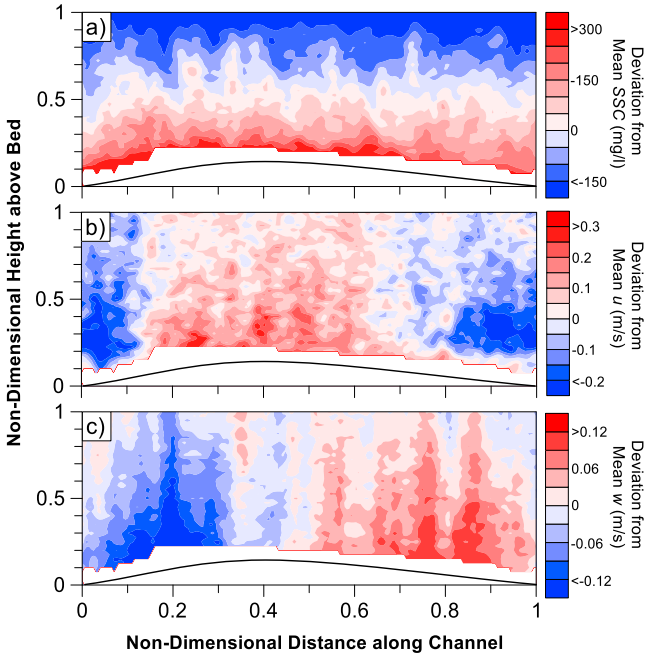

Figure 12. Spatially averaged (a) deviation in suspended sediment concentration from the mean (SSC′), (b) deviation in streamwise velocity from the mean (u'_x), and (c) deviation in vertical velocity from the mean (w'_x). Spatial averages are constructed by normalizing the distance along the dune by the dune length and normalizing the vertical elevation by the flow depth over the 12 largest dunes.

previous two tidal phases. Decreased flow velocity suggests that bed material entrainment had likely stopped and the suspended sediment consisted of finer wash load material.

4. Discussion

4.1. How Does the Flow Structure Over Low-Angle Dunes Change at Different Phases of the Tide?

[39] Observations reported here were made in an estuarine, strongly tidal reach of the Fraser River. The tides imposed significant change in the flow field over the low-angle dunes that dominate this reach of the river. Early in the falling tide, flow was stratified with an upper fresh water layer and a lower saline layer, separated by a mixing layer, but flow within the saline layer was beginning to exit the channel. *MacDonald and Horner-Devine* [2008] and *Tedford et al*. [2009], both working in this reach of the Fraser River, argued that bottom friction retards the outflowing salt wedge, which promotes increased shear along the saline-fresh water interface causing instabilities and increased mixing that we also observed. *Tedford et al*. [2009] showed that asymmetric instabilities were dominantly one-sided Holmboe modes formed along the saline-fresh water interface due to unstable interaction of density and velocity gradients.

[40] During Lower Falling Tide, river flow flushed out the saline water and eliminated stratified flow. Higher WCB′ in the bed form troughs may be related to pockets of salt water previously observed by *Geyer and Farmer* [1989] on falling tides. However, WCB′ in the dune troughs was higher than previously observed at the pycnocline. Others have made the same observation and attributed it to increased near-bed suspended sediment concentration as the salinity intrusion was pushed out of the channel [*Kostaschuk*, 2002; *Kostaschuk and Best*, 2005]. They have reasoned that fine sediment deposited during the near slack water at high tide is readily available for transport as flow in the river begins to accelerate [cf. *Kostaschuk and Best*, 2005].

[41] River flow dominated the channel at low tide. Flow over the low-angle dunes was topographically influenced as flow accelerated over the stoss and decelerated over the lee side. Fluid was forced upward from the lower stoss to the crestal region and moved toward the bed over the lee and trough regions. These topographically induced patterns were consistent throughout the Low Tide transects and agree well with the mean velocity characteristics over low-angle dunes observed by *Kostaschuk and Villard* [1996, 1999] and *Best and Kostaschuk* [2002] These patterns are also similar to the well-documented flow structure over high-angle dunes [e.g., *Nelson et al*., 1993; *McLean et al*., 1994; *Bennett and Best*, 1995; *Venditti and Bennett*, 2000; *Venditti and Bauer*, 2005; *Venditti*, 2013]. The measurements showed no evidence of the flow separation that occurs past the crest over high-angle dunes, in agreement with previous observations that the low-angle lee slopes do not produce permanent flow separation [e.g., *Kostaschuk and Villard*, 1996; *Best and Kostaschuk*, 2002], although aDcp beam geometry may result in spatial averaging volumes too large to capture the separated flow [*Kostaschuk et al*., 2004; *Parsons et al*., 2005]. Highly intermittent near-bed flow reversal, as observed by *Best and Kostaschuk* [2002] over a laboratory dune with a lee side of 14°, may have been occurring in the deceleration zone but was not measured.

[42] At low tide, upwelling occurred where the streamwise velocity decreased as the vertical velocity increased over the trough and lower stoss slope during the Low and Low Rising Tide observations. These motions gave way to positive u and w velocity deviations downstream over the upper stoss slope. Downwelling dominated in the lee of the bed forms and had

slower than the mean u velocity in the immediate lee of the crests and higher than mean u velocity moving over the lee side slope. These upwelling and downwelling motions reflect flow processes that lead to the suspension events.

[43] As the tide began to rise, the decelerated zone of flow in the troughs expanded over the stoss of the next downstream bed form. Regions of upwelling were larger compared to low tide. These observations may represent the enhanced turbulence that occurs in estuaries during rising tides [*Gordon*, 1975; *Kostaschuk et al*., 1989; *Kostaschuk and Best*, 2005] due to variation in longitudinal pressure gradients caused by the tidal flow [*Davies*, 1977]. Alternatively, strong mixing in the low tide flow fields may also have prevented large-scale turbulence production and promoted smaller-scale events that were occurring too frequently to be captured by the aDcp. Patterns in the mean flow became less coherent near high tide until the salt wedge rapidly entered the channel and altered the flow field.

4.2. What Are the Characteristics of Suspension Events at Various Stages of the Tide?

[44] The SSC′ maps during Low (Figure 11a) and Lower Rising (Figure 11b) tide show that flow was dominated by large-scale suspension events that generated sediment concentrations much higher than the ambient flow around them. These events formed near the bed and grew up into the flow as relatively narrow structures at a mean angle of 24°. During low tide, suspension events appeared more numerous than at any other period in the tidal cycle, appearing over all dunes regardless of individual morphological characteristics. *Kostaschuk and Best* [2005] argued that enhanced turbulence on the rising tide may result in increased sediment suspension. Our observations show that, as the tide begins to rise, suspension events emerged as larger structures in the flow, suggesting that turbulence was enhanced; however, suspended sediment concentrations were lower than those at low tide. This suggests that the turbulent events become larger scale, but less energetic, and therefore carry less sediment.

[45] Figure 12a shows a spatial average of SSC′ over the 12 largest dunes in the flow field at low tide. The horizontal and vertical dimensions have been normalized by the dune length and flow depth, respectively. The integrated effect of the suspension events is that there are greater deviations from the mean near the boundary than higher in the flow field. There does not appear, in the figure, to be any location over the dunes where events preferentially occur. This could be interpreted as there being no specific origin for the suspension events over the dunes. However, qualitative examination of the complete data set (all ~1 km long transects) suggests that there are two main regions over the dunes where the suspension events originate: over the trough immediately downstream of the crest and, more frequently, over the lower stoss. Suspension events over the lower stoss were typically low in the water column. Further up over the stoss and crest, events appeared to grow higher up in the water column, as in Figure 11a, suggesting that they were anchored to the bed morphology. Distinct suspension events over the trough immediately downstream of the crest typically appeared as isolated events rather than in a sequence and were not as commonly found over the dunes, indicating that they may have been intermittent. This pattern is not evident in the spatial averages shown in Figure 12a because the structures advect downstream, producing near-equal distributions of deviations from the mean over the dune length.

[46] A direct linkage between the suspension events and a specific fluid structure cannot be made with our data because the sampling volume of the aDcp is too large relative to the structures in order to resolve internal velocities. However, spatially averaged u'_x (Figure 12b) and w'_x (Figure 12c) over the 12 largest dunes do show patterns consistent with persistent upwelling over the trough and lower stoss slope. Strong positive w'_x occurs with a broad region of negative u'_x because the upwelling is bringing slower velocity fluid from the bed vertically to conserve mass. Over the crest of the dunes, where the streamwise deviation from the mean is highest, there is neither upwelling nor downwelling. In the lee of the dune crests, downwelling occurs as the flow begins to decelerate.

[47] The region of strong upwelling over the trough and lower stoss slope is where we observe suspension events to originate in the non–spatially averaged data (e.g., Figure 11a). Previous work has suggested that this upwelling region consists of macroturbulent kolks. *Kostaschuk and Church* [1993], for example, observed suspension events using acoustic water column sounding which they interpreted as macroturbulent kolks that had signatures of ejections and attributed them to upwelling of slower near-bed fluid. Our observations of low concentration deviations (Figure 11a, 24 and 64 m) typically occur in the zones of downwelling.

[48] If these suspension events observed in the SSC′ are large-scale, macroturbulent kolk structures, where they occur over the dunes and their spatial evolution reveal something about the dynamics of kolks. Sediment suspension events that appear over the lower stoss but grow in height over the dunes and dissipate beyond dune crests are consistent with *Best and Kostaschuk*'s [2002] explanation of low-angle dune kolk generation. They suggest that instabilities may form along a weak shear layer between the main flow and decelerated flow in the trough. When these instabilities reach the point of reattachment, they are thought to coalesce into the region of intense upwelling at the lower stoss and grow up into the flow as macroturbulence. The suspension events generated over the trough immediately downstream of the crest may be due to the intermittent flow separation observed by *Best and Kostaschuk* [2002]. However, it is also possible that "burst" events within the turbulent boundary layer [*Jackson*, 1976] grow through the autogeneration of hairpin vortices [*Adrian*, 2007] with no specific point of origin along the dune length. Additional work is required to resolve the origin of coherent structures that emerge over low-angle dunes and flat beds.

4.3. How Much Sediment Is Carried by Suspension Events?

[49] Previous work has qualitatively assessed how large-scale suspension events contribute to sediment flux in rivers, and it is widely accepted that macroturbulent events such as kolks are capable of transporting large volumes of suspended sediment [cf. *Rood and Hickin*, 1989; *Kostaschuk and Church*, 1993; *Kostaschuk and Villard*, 1999; *Venditti and Bennett*, 2000; *Best*, 2005b; *Shugar et al*., 2010]. However, a quantitative understanding of how much large-scale suspension events contribute to sediment flux is absent in the literature. Observations at Low and Lower Rising Tide support the notion that large suspension events are major agents of

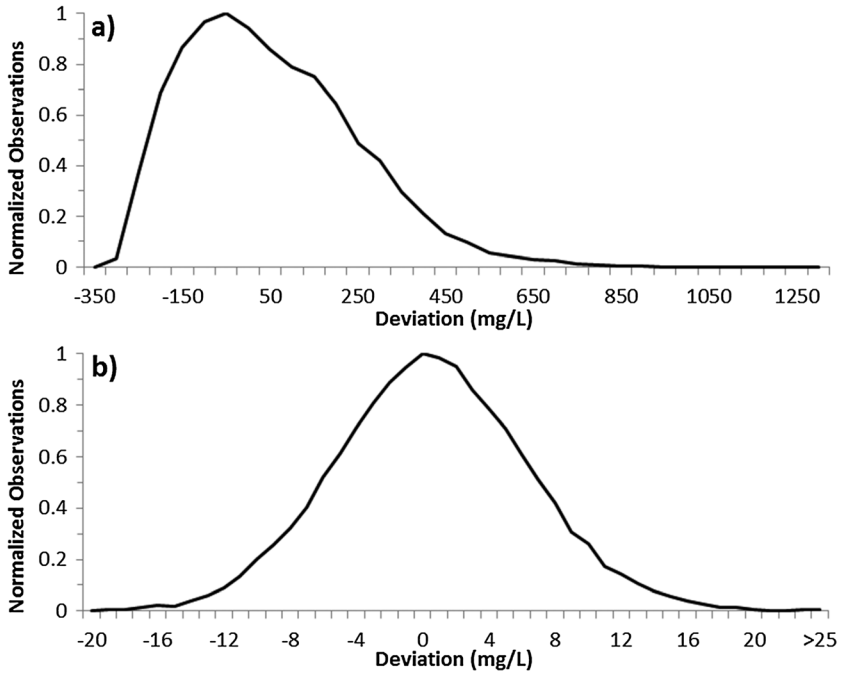

Figure 13. Distribution of the deviation from median suspended sediment concentration observations. (a) Transect M at Low Tide where the flow is dominated by suspension events. (b) Transect K at High Tide when suspended sediment concentrations are low and no events are present in the flow fields. Note the much larger range of deviation values in Figure 13a.

suspended sediment transport. Figure 13 shows the distribution of suspended sediment concentration deviation from the median at low tide (Transect M) and high tide (Transect K). Using the median delineates structures in the same way as the mean but allows for quantitative comparison between different phases of the tide because, by definition, 50% of the flow field is occupied by events with concentrations greater than the median and 50% is not. Figure 13a shows that when suspension events are present over the dunes at Low Tide, the distribution of sediment concentration deviations is skewed toward higher concentrations. When the well-defined suspension events are absent at High Tide, the observations are normally distributed (Figure 13b). Figure 13a shows that high concentrations are carried in a smaller total volume over the dunes at low tide.

[50] The suspended sediment concentration fields allow us to further quantify how much sediment is carried by suspension events. For each transect, we calculated the volume of sediment in suspension (V) by summing the volume of sediment carried in each cell:

$$V = \sum C_i h_i l_i w_i, \tag{19}$$

where C_i is the suspended sediment concentration in each cell (in mg/m^3) and where cells have a height $h_i = 0.25$ m, a length l_i equal to the average distance between ensembles for the transect, and a width w_i assumed to be 1 m (a unit width). We first used equation (19) to calculate the total sediment volume in suspension, V_T. Then we calculated the volume in cells that had concentrations greater than the median $V_{>M}$. Changes in the ratio of $V_{>M}/V_T$ highlight the way that suspension events affect sediment concentrations in the channel. Care needs to be taken when interpreting this calculation.

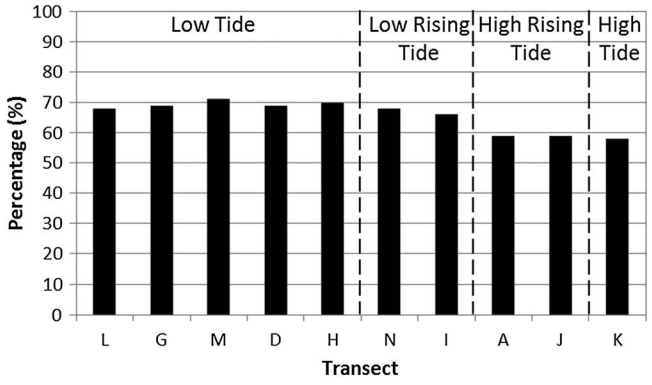

Figure 14. The percentage of sediment volume carried in cells with concentrations greater than the median ($V_{>M}$) relative to the sum of the total sediment volume (V_T).

Suspension events will tend to increase the bed material concentration in the flow, so without separating bed material from wash material, we cannot calculate the amount of bed material suspended by an individual event without making some assumptions about the cell-specific wash material load. We also need to be careful near the bed because some cells may have bed material in suspension that is not associated with these events. Nevertheless, an examination of $V_{>M}/V_T$ reveals the effect of large suspension events in the flow relative to when they are absent.

[51] Figure 14 shows the ratio of the volume of sediment carried in cells with concentrations greater than the median $V_{>M}$ relative to V_T. At Low Tide, when the flow is dominated by suspension events, ~69% of the total sediment is carried in 50% of the flow. As tides begin to rise and suspension events become less frequent but are more easy to identify, $V_{>M}/V_T$ was 67%. When clearly defined events stop emerging over the dunes at High Rising and High Tide, but finer sediment is likely still in suspension, 59% of the total sediment is carried in 50% of the flow. While the amount carried in the flow is positively skewed for all of the transects (e.g., Figure 13), these results suggest that more sediment is carried in a smaller volume of water at low tides than at higher tides, quantitatively indicating that these suspension events are indeed responsible for a large portion of the sediment in suspension.

[52] While Figure 14 provides a quantitative measure of how sediment suspension events affect the volume of sediment transported in the channel, further work needs to focus on grain size separation of bed material (sand) and wash load (silt-clay) within the water column to determine how much sediment flux can be attributed to individual suspension events. However, better event detection and identification methods are needed as well, which will require new instrumentation with smaller sampling volumes than the aDcp to properly resolve the fluid signatures of individual suspension events. Nevertheless, the difference observed in the proportion of sediment carried above the median, with and without suspension events, provides quantitative evidence of their effect on sediment concentrations over low-angle dunes.

5. Conclusions

[53] Mean flow and suspension events in variable flow were examined in a tidally influenced reach of the Fraser River, British Columbia, Canada. Dunes displayed low-angle (12° on average) lee sides typical of dunes in large, tidally influenced sand-bedded rivers and estuaries rather than the angle-of-repose asymmetric geometry typical of small channels and flumes. Flow and suspended sediment transport patterns were variable through tidal cycles, but reoccurring patterns showed the following:

[54] 1. At high tide, saline water entered the channel and saline plumes of water were forced up over the dunes into the downstream-moving fresh water due to topographic forcing. The salt wedge persisted in the channel, promoting stratified flow with instabilities forming along the saline-fresh water interface.

[55] 2. As tides approached the minimum stage, river processes dominated over the salt wedge and forced the saline water out of the channel. Velocity and suspended sediment concentrations peaked at low tide but decreased as the tides rose.

[56] 3. Observations of flow over the low-angle dunes displayed patterns of topographic forcing similar to those observed over high-angle dunes. However, unlike flow over high-angle dunes, we found no evidence of separated flow or flow reversal.

[57] 4. Velocity records showed upwelling over the dune trough and lower stoss slopes and downwelling over the bed form crest and lee slope.

[58] 5. Large-scale suspension events emerged in the suspended sediment records during low and rising tides. Discrete events dominated the suspended sediment fields at low tide and became less frequent but larger scale as the tide began to rise.

[59] 6. Suspension events emerged over the lower stoss side of dunes and grew up over the bed forms and also formed immediately downstream of the crest, although less commonly.

[60] 7. The suspension events carry more sediment than the ambient fluid over dunes. We estimate that 69% of the total sediment is carried by 50% of the flow during low tide when suspension events dominate.

[61] These results illustrate how the mean flow field changes over low-angle dunes in variable flow associated with tidal cycles, reveal patterns of suspension events over low-angle dunes, and show that these events are important in sediment transport. These observations substantially extend prior results on flow over the low-angle dunes in the Fraser Estuary [*Kostaschuk*, 2000, 2002; *Kostaschuk et al*., 1989; *Kostaschuk and Church*, 1993; *Kostaschuk and Villard*, 1996, 1999; *Villard and Church*, 2003; *Kostaschuk and Best*, 2005; *Kostaschuk et al*., 2010] in as much as those studies were mainly restricted to the documentation of mean flows and mean sediment concentration in the dune field. The most recent studies have deployed aDcp instruments but have not succeeded in resolving sediment plumes well or to associate them with individual flow structures. The demonstration in this study substantially narrows the range of possible mechanisms by which sediment mobilization occurs at different phases of the tide in a large estuary. It is clear that still more highly resolved measurements are required—in particular of the velocity field—before a firm theoretical approach can be made to the problem, but this study clearly indicates the nature of the required measurements. Future work must be coupled with controlled flume experiments and numerical simulations in order to resolve the origin of coherent structures at finer scales and to determine how these structures interact with the bed to suspend bed material.

[62] **Acknowledgments.** This work was supported by the National Sciences and Engineering Research Council of Canada (NSERC) Discovery grants to J.G.V., R.A.K., and M.C. R.W.B. was supported by a NSERC Alexander Graham Bell Canada Graduate Scholarship. Technical support and field assistance were kindly provided by Dan Duncan (UT), Maureen Attard (SFU), and Sally Haggarstone (SFU).

References

Adrian, R. J. (2007), Hairpin vortex organization in wall turbulence, *Phys. Fluids*, *19*, 041301, doi:10.1063/1.2717527.

Allen, J. R. L. (1982), *Sedimentary Structures: Their Character and Physical Basis*, Elsevier, New York, N. Y.

Attard, M. E. (2012), Evaluation of aDcps for suspended sediment transport monitoring: Fraser River, British Columbia. M.Sc. thesis, pp. 118, Dept. Geog., Simon Fraser Univ., Burnaby, British Columbia, Canada.

Babakaiff, C. S., and E. J. Hickin (1996), Coherent flow structures in Squamish River Estuary, British Columbia, Canada, in *Coherent Flow*

Structures in Open Channels, edited by P. J. Ashworth et al., John Wiley, Hoboken, N. J., pp. 321–342.

Bennett, S. J., and J. L. Best (1995), Mean flow and turbulence structure over fixed, two-dimensional dunes: Implications for sediment transport and bedform stability, *Sedimentology*, *42*, 491–513.

Best, J. L. (2005a), The fluid dynamics of river dunes: A review and some future research directions, *J. Geophys. Res.*, *110*, F04S02, doi:10.1029/2004JF000218.

Best, J. L. (2005b), The kinematics, topology and significance of dune related macroturbulence: Some observations from the laboratory and field, in *Fluvial Sedimentology VII. Special Publication*, Spec. Publ. Int. Assoc. Sedimentol., edited by M. D. Blum, S. B. Marriott, and S. Leclair, vol. *35*, pp. 41–60, Blackwell, Malden, Mass.

Best, J. L., and R. A. Kostaschuk (2002), An experimental study of turbulent flow over a low-angle dune, *J. Geophys. Res.*, *107*(C9), 3135, doi:10.1029/2000JC000294.

Coleman, J. M. (1969), Brahmaputra River: Channel processes and sedimentation, *Sedimentary Geology.*, *3*, 129–239.

Davies, A. G. (1977), A mathematical model of sediment in suspension in a uniform reversing tidal flow, *Geophys. J. R. Astron. Soc.*, *51*, 503–529, doi:10.1111/j.1365-246X.1977.tb06932.x.

Domarad, N. (2011), Flow and suspended sediment transport through the gravel-sand transition in the Fraser River, British Columbia. M.Sc. thesis, 110 pp., Dept. Geog., Simon Fraser Univ., Burnaby, British Columbia, Canada.

Gartner, J. W. (2004), Estimating suspended solids concentrations from backscatter intensity measured by acoustic Doppler current profiler in San Francisco Bay, California, *Mar. Geol.*, *211*, 169–187, doi:10.1016/j.margeo.2004.07.001.

Geyer, W., and D. Farmer (1989), Tide-induced variation of the dynamics of a salt wedge estuary, *J. Phys. Oceanogr.*, *19*, 1060–1672.

Gordon, C. M. (1975), Sediment entrainment and suspension in a tidal flow, *Mar. Geol.*, *18*, 57–64, doi:10.1016/0025-3227(75)90040-7.

Jackson, R. G. (1976), Sedimentological and fluid-dynamic implications of the turbulence bursting phenomenon in geophysical flows, *J. Fluid Mech.*, *77*, 531–560.

Kostaschuk, R. A. (2000), A field study of turbulence and sediment dynamics over subaqueous dunes with flow separation, *Sedimentology*, *47*, 519–531.

Kostaschuk, R. A. (2002), Flow and sediment dynamics in migrating salinity intrusions: Fraser River estuary, Canada, *Estuaries*, *25*(2), 197–203.

Kostaschuk, R., and J. Best (2005), Response of sand dunes to variations in tidal flow: Fraser Estuary, Canada, *J. Geophys. Res.*, *110*, F04S04, doi:10.1029/2004JF000176.

Kostaschuk, R. A., and M. A. Church (1993), Macroturbulence generated by dunes: Fraser River, Canada, *Sediment. Geol.*, *85*, 25–37.

Kostaschuk, R. A., and P. V. Villard (1996), Flow and sediment transport over large subaqueous dunes: Fraser River, Canada, *Sedimentology*, *43*, 849–863.

Kostaschuk, R. A., and P. V. Villard (1999), Turbulent sand suspension over dunes, in *Fluvial Sedimentology VI*, edited by N. D. Smith and J. Rogers, *Spec. Publ. Int. Assoc. Sedimentol*., *28*, 3–14.

Kostaschuk, R. A., M. A. Church, and J. L. Luternauer (1989), Bed-material, bedforms and bed load in a salt-wedge estuary Fraser River, British Columbia, *Can. J. Earth Sci.*, *26*, 1440–1452.

Kostaschuk, R. A., P. V. Villard, and J. L. Best (2004), Measuring velocity and shear stress over dunes with an acoustic Doppler profiler, *J. Hydraul. Eng.*, *130*, 932–936.

Kostaschuk, R. A., J. L. Best, and P. V. Villard (2010), The influence of dunes on mixing in a migrating salt-wedge: Fraser River estuary, Canada, *Earth Surf. Process. Landforms*, *35*, 460–465, doi:10.1002/esp.1928.

MacDonald, D., and A. Horner-Devine (2008), Temporal and spatial variability of vertical salt flux in a highly stratified estuary, *J. Geophys. Res.*, *113*, C09022, doi:10.1029/2007JC004620.

Mark, D. M., and M. A. Church (1977), On the misuse of regression in earth science, *Math. Geol.*, *9*, 63–75, doi:10.1007/BF02312496.

Matthes, G. M. (1947), Macroturbulence in natural stream flow, *EOS, Transactions, American Geophysical Union*, *28*, 255–263.

McLaren, P., and P. Ren. (1995), Sediment transport and its environmental implications in the Lower Fraser River and Fraser Delta, in *Canada Department of Environment, Environmental Conservation, DOE FRAP* 1995-03, p. 37.

McLean, S. R., J. M. Nelson, and S. R. Wolfe (1994), Turbulence structure over two-dimensional bedforms: Implications for sediment transport, *J. Geophys. Res.*, *99*, 12,729–12,747.

McLean, D. G., M. A. Church, and B. Tassone (1999), Sediment transport along lower Fraser River. 1. Measurements and hydraulic computations, *Water Resour. Res.*, *35*, 2533–2548, doi:10.1029/1999WR900101.

Müller, A., and A. Gyr (1986), On the vortex formation in the mixing layer behind dunes, *J. Hydraul. Res.*, *24*, 359–375.

Nelson, J. M., S. R. McLean, and S. R. Wolfe (1993), Mean flow and turbulence fields over two-dimensional bedforms, *Water Resour. Res.*, *29*, 3935–3953.

Nezu, I., and H. Nakagawa (1993), *Turbulence in Open-Channel Flows*, 281 pp., A. A. Balkema, Brookfield, Vt.

Omidyeganeh, M., and U. Piomelli (2011), Large-eddy simulation of two dimensional dunes in a steady, unidirectional flow, *J. Turbul.*, *12*(42), 1–31.

Parsons, D. R., J. L. Best, O. Orfeo, R. J. Hardy, R. A. Kostaschuk, and S. N. Lane (2005), The morphology and flow fields of three-dimensional dunes, Rio Paraná, Argentina: Results from simultaneous multibeam echo sounding and acoustic Doppler current profiling, *J. Geophys. Res.*, *110*, F04S03, doi:10.1029/2004JF000231.

Rennie, C. D., and M. A. Church (2010), Mapping spatial distributions and uncertainty of water and sediment flux in a large gravel bed river reach using an acoustic Doppler current profiler, *J. Geophys. Res.*, *115*, F03035, doi:10.1029/2009JF001556.

Rennie, C. D., and F. Rainville (2006), Case study of precision of GPS differential correction strategies: Influence on aDcp velocity and discharge estimates, *J. Hydraul. Eng.*, *132*, 225–234, doi:10.1061/(ASCE)0733-9429(2006)132:3(225).

Rennie, C. D., F. Rainville, and S. Kashyap (2007), Improved estimation of ADCP apparent bed-load velocity using a real-time Kalman filter, *J. Hydraul. Eng.*, *133*, 1337–1344, doi:10.1061/(ASCE)0733-9429(2007).

Reson Inc. (2009), SeaBat 7101 High-Resolution Multibeam Echosounder System Operator's Manual, Denmark.

Roden, J. E. (1998), The sedimentology and dynamics of mega-dunes, Jamuna River, Bangladesh, Ph.D. thesis, 310 pp., Dep. of Earth Sci., Univ. of Leeds, Leeds, U. K.

Rood, K. M., and E. J. Hickin (1989), Suspended sediment concentration in relation to surface-flow structure in Squamish River estuary, southwestern British Columbia, *Can. J. Earth Sci.*, *26*, 2172–2176.

Schulkin, M., and H. W. Marsh (1962), Sound absorption in sea water, *J. Acoust. Soc. Am.*, *34*(6), 864–865.

Shugar, D. H., R. A. Kostaschuk, J. L. Best, D. R. Parsons, S. N. Lane, O. Orfeo, and R. J. Hardy (2010), On the relationship between flow and suspended sediment transport over the crest of a sand dune, Río Paraná, Argentina, *Sedimentology*, *57*, 252–272, doi:10.1111/j.1365-3091.2009.01110.x.

Smith, J. D., and S. R. McLean (1977), Spatially averaged flow over a wavy surface, *J. Geophys. Res.*, *82*, 1735–1746.

Tedford, E. W., J. R. Carpenter, R. Pawlowicz, R. Pieters, and G. A. Lawrence (2009), Observation and analysis of shear instability in the Fraser River estuary, *J. Geophys. Res.*, *114*, C11006, doi:10.1029/2009JC005313.

Teledyne RD Instruments (2001), WorkHorse Monitor ADCP User's Guide, San Diego, Calif.

Topping, D. J., S. A. Wright, T. S. Melis, and D. M. Rubin (2007), High-resolution measurements of suspended-sediment concentration and grain size in the Colorado River in Grand Canyon using a multi-frequency acoustic system, in Proceedings of the 10th International Symposium on River Sedimentation, August 1–4, Moscow, Russia.

Venditti, J. G. (2013), Bedforms in sand-bedded rivers, in *Treatise on Geomorphology*, Fluvial Geomorphology, vol. *9*, edited by J. F. Shroder (Editor-in-chief), E. Wohl, pp. 137–162, (Volume Editor), Academic Press, San Diego.

Venditti, J. G., and B. O. Bauer (2005), Turbulent flow over a dune: Green River, Colorado, *Earth Surf. Process. Landforms*, *30*, 289–304, doi:10.1002/esp.1142.

Venditti, J. G., and S. J. Bennett (2000), Spectral analysis of turbulent flow and suspended sediment transport over fixed dunes, *J. Geophys. Res.*, *105*, 22,035–22,047.

Villard, P. V., and M. Church (2003), Dunes and associated sand transport in a tidally influence sand-bed channel: Fraser River, British Columbia, *Can. J. Earth Sci.*, *40*, 115–130.

Wright, S. A., D. J. Topping, and C. A. Williams (2010), Discriminating silt-and-clay from suspended sand in rivers using side-looking acoustic profilers, in 2nd Joint Federal Interagency Conference, July 24-June 1, Las Vegas, Nevada, USA.